Optics Letters

p-type doping of MgZnO films and their applications in optoelectronic devices

C. X. Shan,[1,2,5] J. S. Liu,[1,3] Y. J. Lu,[1] B. H. Li,[1] Francis C. C. Ling,[4] and D. Z. Shen[1,6]

[1]State Key Laboratory of Luminescence and Application, Changchun Institute of Optics, Fine Mechanics and Physics, Chinese Academy of Sciences, Changchun 130033, China
[2]School of Physical Engineering, Zhengzhou University, Zhengzhou 450052, China
[3]State Key Laboratory of Functional Materials for Informatics, Shanghai Institute of Microsystem and Information Technology, Chinese Academy of Sciences, Shanghai 200050, China
[4]Department of Physics, The University of Hong Kong, Pokfulam Road, Hong Kong, China
[5]e-mail: shancx@ciomp.ac.cn
[6]e-mail: shendz@ciomp.ac.cn

Received 12 May 2015; accepted 20 May 2015; posted 4 June 2015 (Doc. ID 240834); published 22 June 2015

A lithium and nitrogen codoping method has been employed to prepare *p*-type MgZnO films, and *p*-MgZnO/*i*-ZnO/*n*-ZnO structured light-emitting devices (LEDs) and photodetectors have been fabricated. The LEDs can work continuously for about 97 h under the injection of a 20 mA continuous current, which is the best value ever reported for ZnO-based LEDs. The performance of the photodetectors degrades little after several running cycles. The above results reveal the applicability of the *p*-MgZnO films in optoelectronic devices.

OCIS codes: (310.6845) Thin film devices and applications; (260.3800) Luminescence; (230.3670) Light-emitting diodes; (040.5160) Photodetectors.

http://dx.doi.org/10.1364/OL.40.003041

Zinc oxide (ZnO) has long been regarded as a promising candidate for applications in ultraviolet (UV) optoelectronic devices, including light-emitting devices (LEDs) and photodetectors [1,2]. Because of the above potential applications, much attention has been paid to this material in the past decades [3–5]. One of the most challenging issues of ZnO lies in the difficulty of realizing efficient *p*-type conduction. Although quite a few reports claimed the realization of *p*-type ZnO films, and some optoelectronic devices have been demonstrated [6–8], the performance of such devices is still far below expectation. It is accepted that heterostructures constituted by alloyed semiconductor with different compositions can ensure efficient carrier injection and confinement, and thus may help to realize high-performance optoelectronic devices. MgZnO has been regarded as an ideal counterpart of ZnO [9,10]. To realize MgZnO/ZnO heterostructures, *p*-type doping of MgZnO is indispensible in some cases. Considering its wider bandgap, the *p*-type doping of MgZnO may be more challenging. In fact, the report on the *p*-type doping of MgZnO is still rare although it is eagerly wanted [11–14].

Reproducible and stable *p*-ZnO films have been realized by employing a lithium and nitrogen codoping method in our previous publication [15–18]. In this Letter, we show that by employing the Li, N codoping method, *p*-MgZnO films can be obtained, and *p*-MgZnO/*i*-ZnO/*n*-ZnO structured LEDs and photodetectors have been constructed. The LEDs can work continuously for about 97 h, and the photodetectors show little degradation after several running cycles, indicating the applicability of the *p*-MgZnO films in optoelectronic devices.

The *p*-type doping of MgZnO films was carried out in a VG V80H plasma-assisted molecular beam epitaxy technique on *a*-plane sapphire by employing nitric oxide as N and O sources, and elemental Zn, Mg, and Li in individual Knudsen cells as other precursors. During the growth process, the pressure in the growth chamber was fixed at 2×10^{-5} mbar and the substrate temperature at 700°C. The crystal structure of the films was studied in a Bruker D8 x-ray diffractometer (XRD) using CuKα ($\lambda = 1.54$ Å) as the excitation source. The electrical properties of the films were characterized by Hall measurement (Lakeshore 7707) under van der Pauw configuration. An AXIS Ultra^{DLD} x-ray photoelectron spectroscope (XPS) has been employed to determine the chemical bonding state and doping concentration of the films. Electroluminescence (EL) measurements were carried out in a Hitachi F4500 spectrometer under the drive of continuous current. The response of the photodetectors was characterized using a lock-in amplifier, a Spex scanning monochromator, and a 150 W Xe lamp was employed as the illumination source. The temporal response of the photodetector was measured under the excitation of the 266 nm line of an Nd:YAG laser with the output power of around 1 mW.

Figure 1(a) shows the XPS spectrum of the MgZnO:(Li,N) films; note that the spectrum has been adjusted based on the standard C 1s peak at 284.6 eV. All the obvious peaks in the survey spectrum can be attributed to Zn, Mg, and O; the Mg content in the MgZnO films determined by the XPS spectrum

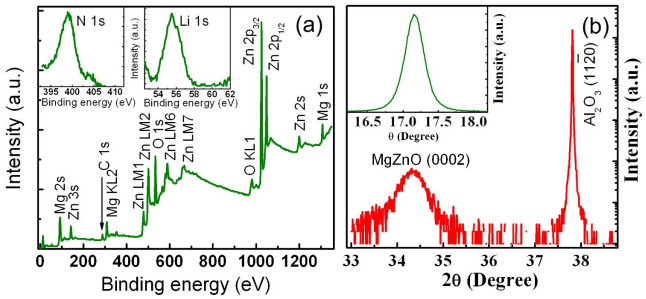

Fig. 1. (a) Survey XPS spectrum of the MgZnO:Li,N films; the inset shows the XPS spectra of N 1s and Li 1s in the MgZnO:(Li, N) films. (b) XRD pattern of the MgZnO films grown on sapphire substrate; the inset shows the rocking curve of the films.

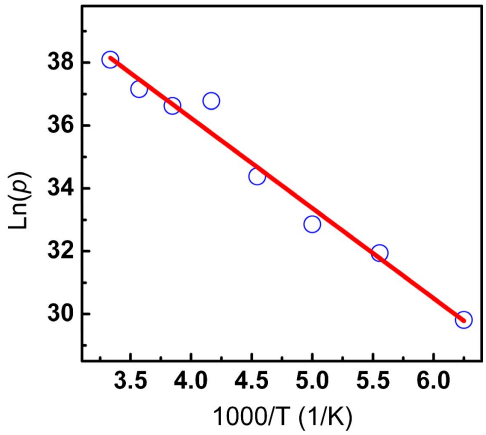

Fig. 2. Temperature-dependent hole concentration of the MgZnO:(Li,N) films obtained by Hall measurement; the solid line is a fitting to the scattered experimental data.

is around 17%; and the atomic concentration of Li and N in the films is around 1.84% and 0.43%. A detailed investigation shows two peaks at around 55.4 and 399.1 eV, as illustrated in the inset of Fig. 1(a), which can be attributed to the 1s peak of Li and N. The peak at around 399.1 eV is very close to the Li–N bonds in lithium azide (399.3 eV) [19,20]; thus, it can be assigned to the N 1s of Li–N bonds in our case. The Li 1s peak at 55.4 eV lies between the binding energy of Li–O (55.6 eV) [21] and Li–N bonds (55.2 eV) [19]; thus, the Li may bond with O or N in the MgZnO films. From the above discussion, it is clear that Li and N have been incorporated into the MgZnO films. The structural properties of the $Mg_{0.17}Zn_{0.83}O$:(Li, N) films assessed by XRD are indicated in Fig. 1(b). The XRD pattern shows two peaks at around 34.38° and 37.82°; the former can be attributed to the diffraction from the (0002) facet of $Mg_{0.17}Zn_{0.83}O$, and the latter to the *a*-plane sapphire. Note that the origin for the (0001) orientation of ZnO on *a*-plane sapphire can be attributed to the matchup of the atomic arrangement on these two surfaces [22]. The x-ray rocking curve of the MgZnO film is shown in the inset of Fig. 1(b). A Gaussian curve with a full width at half-maximum of 0.3° is visible from the figure.

Hall measurement on the $Mg_{0.17}Zn_{0.83}O$:(Li, N) films reveals that the films display *p*-type conductivity, and the room temperature hole concentration and Hall mobility of the films are 3.6×10^{16} cm^{-3} and 3.2 $cm^2\,V^{-1}\,s^{-1}$, respectively. Temperature dependent Hall measurement on the $Mg_{0.17}Zn_{0.83}O$:(Li, N) films have also been carried out, as illustrated in Fig. 2. It is found that the hole concentration increases gradually with temperature. The phenomenon is rational since more acceptors will be activated by the thermal energy at elevated temperature, and the activation energy of the acceptors (E_A) can be derived from the dependence of the hole concentration (p) on temperature using the following formula [23]:

$$p = ((N_A - N_D)N_v/2N_D)\exp(-E_A/k_BT), \quad (1)$$

where N_A is the acceptor concentration, N_D is the compensating donor concentration, N_V is the effective density of states in the valance band, k_B is the Boltzmann constant, and T is Kelvin temperature. By fitting the experimental data using Eq. (1), an activation energy of 211 meV can be derived. We note that this value is significantly larger than the corresponding theoretical (90 meV) [24] and experimental (80 meV) [14] value obtained for ZnO:(Li,N). We think the increased activation energy for acceptors in MgZnO compared with that in ZnO is rational, since the bandgap has been widened with the incorporation of Mg. The *p*-type conductivity in the $Mg_{0.17}Zn_{0.83}O$:(Li, N) may result from the nitrogen on oxygen sites, lithium on zinc sites, or Li–N complex.

To test the applicability of the *p*-$Mg_{0.17}Zn_{0.83}O$ films in optoelectronic devices, *p*-$Mg_{0.17}Zn_{0.83}O$:(Li, N)/*i*-ZnO/*n*-ZnO structure LEDs have been constructed, and the schematic diagram of the LEDs is shown in the inset of Fig. 3. In this structure, the *n*-ZnO is 500 nm in thickness with an electron concentration of 1.4×10^{19} cm^{-3} and a Hall mobility of 42 $cm^2\,V^{-1}\,s^{-1}$. The undoped ZnO (*i*-ZnO) film is 15 nm in thickness, and the electron concentration and Hall mobility of this layer is 3.0×10^{17} cm^{-3} and 56 $cm^2\,V^{-1}\,s^{-1}$, respectively. The thickness of the *p*-MgZnO layer is around 90 nm. The current–voltage (I-V) curve of the structure shows an obvious rectifying behavior with a turn-on voltage of around 6.2 V, as indicated in Fig. 3.

Under forward bias, emissions can be detected from the *p*-$Mg_{0.17}Zn_{0.83}O$:(Li, N)/*i*-ZnO/*n*-ZnO structures, and the EL spectra are shown in Fig. 4. The spectra show a dominant emission at around 390 nm, which comes from the excitonic near-band-edge (NBE) emission of ZnO [25]. With increasing

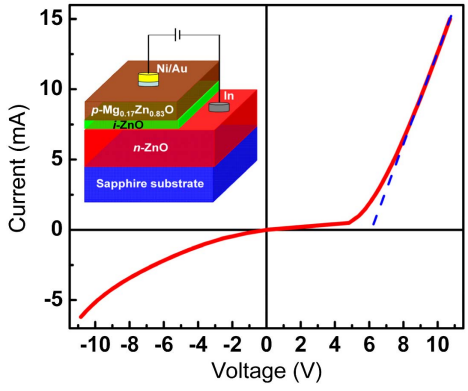

Fig. 3. I-V curve of the *p*-MgZnO:(Li, N)/*i*-ZnO/*n*-ZnO structure. The inset shows a schematic illustration of the structure.

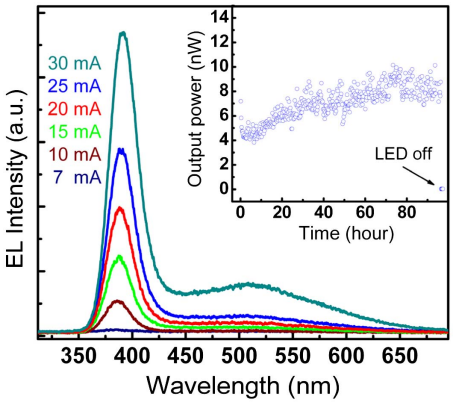

Fig. 4. Room temperature EL spectra of the structure under different injection current. The inset shows the output power of the LED as a function of its running time under the injection of a 20 mA current; note that the last scatter symbol indicates the emission intensity when the LED is switched off.

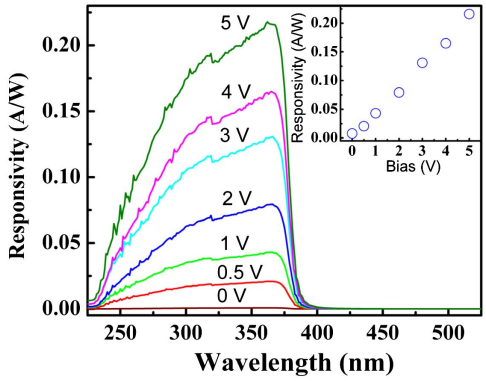

Fig. 5. Response spectra of the *p*-MgZnO:(Li, N)/*i*-ZnO/*n*-ZnO structure at different negative bias. The inset shows the maximum responsivity of the structure as a function of the bias applied.

current, the EL intensity increases gradually. Note that the visible emission at around 500 nm, which is usually attributed to deep-level related emission of ZnO, is much weaker than the NBE emission. The emission mechanism of the *p*-$Mg_{0.17}Zn_{0.83}O$:(Li, N)/*i*-ZnO/*n*-ZnO structures can be understood as follows: When the structure is forward biased, holes in the *p*-$Mg_{0.17}Zn_{0.83}O$ will be injected into the *i*-ZnO layer, while electrons will also be injected into this layer from the *n*-ZnO. As a result, electrons and holes will recombine in the *i*-ZnO layer; thus, emission from this layer can be detected. Thanks to the relatively high quality of the *i*-ZnO layer, the NBE emission dominates the EL spectra while the deep level emission is weak.

To assess the reliability of the devices, a continuous-wave current of 20 mA was injected into the LEDs continuously, and the emission intensity of the LEDs was recorded periodically by a power meter, the result of which is shown in the inset of Fig. 4. One can see that the output power of the LEDs is around several nanowatts. The output power decreases initially, then shows almost no degradation at longer operation duration. Note that the output power fluctuations may be resulted from the re-equalization of the carriers under the heating effect caused by the injection current. The LEDs can still work after around 97 h; this is the longest lifetime ever reported for ZnO-based LEDs [25–28], indicating good reliability of the devices.

Another important potential application of ZnO is the UV photodetector, and many types of ZnO-based photodetectors including metal–semiconductor–metal [29], photoconductive [30], Schottky [31], and *p-n* junctions [17,18], have been demonstrated in the past decades. Among the above types, *p-n* junctions have been considered as one of the most promising structures for high-performance photodetectors with both high responsivity and fast response speed, which are two of the most important parameters that determine the figure-of-merit of a photodetector. However, the report on ZnO *p-n* junction UV photodetectors is still limited [17,18]. On the basis of realizing reliable *p*-type $Mg_{0.17}Zn_{0.83}O$ films, a UV photodetector has been fabricated from the *p*-$Mg_{0.17}Zn_{0.83}O$:(Li, N)/*i*-ZnO/*n*-ZnO structures. Under the illumination of UV light, electrons and holes will be generated in the $Mg_{0.17}Zn_{0.83}O$ and ZnO layers. Under negative bias conditions, the photo generated minority carriers in the *p*-$Mg_{0.17}Zn_{0.83}O$ and *n*-ZnO will drift toward the opposite side and be collected by the electrode there. In this way, the structure will show response to UV light. The response spectra of the structure under different negative bias are shown in Fig. 5. One can see that all the spectra show the same line-shape with a maximum responsivity at around 362 nm, and a cutoff wavelength at around 379 nm. Note that the responsivity of the photodetector is dominated by ZnO because its thickness is much larger than that of MgZnO. Note that the peak responsivity of the photodetector is 7.8×10^{-4} A/W at 0 V bias, while it increases linearly to 0.22 A/W when the bias is 5 V, as shown in the inset of Fig. 5.

Response speed is another important parameter for a photodetector. The temporal response of the *p*-$Mg_{0.17}Zn_{0.83}O$:(Li, N)/*i*-ZnO/*n*-ZnO structure photodetector has been measured, and the results are shown in Fig. 6. In this figure, the rise time of the photodetector is about 0.32 ms, while the decay data can be well fitted using a two-order exponential formula, and the best fitting yields $\tau_1 = 0.29$ ms and $\tau_2 = 7.24$ ms. The above results confirm that there are two decay channels in the photodetector, and the fast one may come from the *p-i-n* structure, while the slow one from the carrier trapping at the Ni/Au contacts on the MgZnO films. Note that

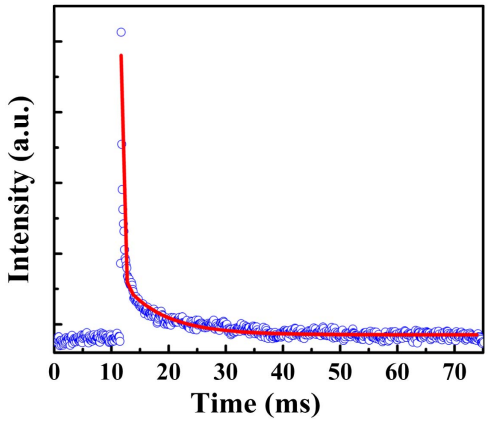

Fig. 6. Temporal response of the UV photodetector, in which the scattered circles are experimental data. The solid line is a fitting to the experimental data using a two-order exponential decay expression.

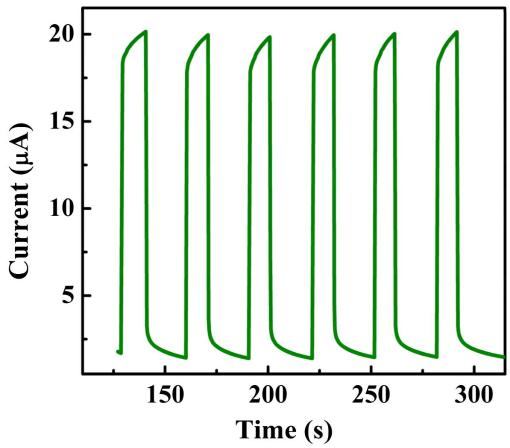

Fig. 7. Time-resolved photocurrent of the photodetector with UV light on and off repeatedly.

ZnO photodetectors with two decay channels have been reported frequently before [31,32].

To test the reliability of the *p*-$Mg_{0.17}Zn_{0.83}O$:(Li, N)/*i*-ZnO/*n*-ZnO structure photodetector, time-resolved photocurrent of the device has been measured with the illumination UV light on and off repeatedly, and the results of which are shown in Fig. 7. One can see from the figure that the device shows little degradation in the investigated timescale, indicating the good reliability of the photodetector.

In summary, *p*-type $Mg_{0.17}Zn_{0.83}O$ films have been realized by employing Li,N codoping method. To test the applicability of the *p*-type films in optoelectronic devices, *p*-$Mg_{0.17}Zn_{0.83}O$:(Li, N)/*i*-ZnO/*n*-ZnO structure LEDs and UV photodetectors have been fabricated. The LEDs can work continuously for around 97 h, and the performance of the UV photodetectors shows little degradation after six running cycles, indicating the good reliability of the *p*-MgZnO films. The results reported in this Letter reveal that Li,N codoping may be a promising route to *p*-type MgZnO; thus may address a step toward ZnO-based heterostructure optoelectronic devices.

National Basic Research Program of China (2011CB302005, 2011CB302006); National Science Foundation for Distinguished Young Scholars of China (61425021); National Natural Science Foundation of China (11374296, 61177040, 61475153).

REFERENCES

1. D. C. Look, Mater. Sci. Eng. B **80**, 383 (2001).
2. U. Ozgur, Y. I. Alivov, C. Liu, A. Teke, M. A. Reshchikov, S. Dogan, V. Avrutin, S. J. Cho, and H. Morkoc, J. Appl. Phys. **98**, 041301 (2005).
3. A. Tsukazaki, T. Onuma, M. Ohtani, T. Makino, M. Sumiya, K. Ohtani, S. F. Chichibu, S. Fuke, Y. Segawa, H. Ohno, H. Koinuma, and M. Kawasaki, Nat. Mater. **4**, 42 (2005).
4. S. J. Jiao, Z. Z. Zhang, Y. M. Lu, D. Z. Shen, B. Yao, J. Y. Zhang, B. H. Li, D. X. Zhao, X. W. Fan, and Z. K. Tang, Appl. Phys. Lett. **88**, 031911 (2006).
5. J. H. Lim, C. K. Kang, K. K. Kim, I. K. Park, D. K. Hwang, and S. J. Park, Adv. Mater. **18**, 2720 (2006).
6. S. Heitsch, G. Benndorf, G. Zimmermann, C. Schulz, D. Spemann, H. Hochmuth, H. Schmidt, T. Nobis, M. Lorenz, and M. Grundmann, Appl. Phys. A **88**, 99 (2007).
7. S. Chu, J. Zhao, Z. Zuo, J. Kong, L. Li, and J. L. Liu, J. Appl. Phys. **109**, 123110 (2011).
8. R. Vidya, P. Ravindran, and H. Fjellvag, J. Appl. Phys. **111**, 123713 (2012).
9. S. J. Pearton, *GaN and ZnO-Based Materials and Devices* (Springer, 2013), p. 413.
10. A. Ohtomo, M. Kawasaki, T. Koida, K. Masubuchi, H. Koinuma, Y. Sakurai, Y. Yoshida, T. Yasuda, and Y. Segawa, Appl. Phys. Lett. **72**, 2466 (1998).
11. Z. P. Wei, B. Yao, Z. Z. Zhang, Y. M. Lu, D. Z. Shen, B. H. Li, X. H. Wang, J. Y. Zhang, D. X. Zhao, X. W. Fan, and Z. K. Tang, Appl. Phys. Lett. **89**, 102104 (2006).
12. A. Y. Polyakov, N. B. Smirnov, A. V. Govorkov, E. A. Kozhukhova, A. I. Belogorokhov, H. S. Kim, D. P. Norton, and S. J. Pearton, J. Appl. Phys. **103**, 083704 (2008).
13. X. Dong, Y. B. Liu, K. K. Huang, W. Zhao, Y. Ye, X. C. Xia, Y. T. Zhang, J. Wang, B. L. Zhang, and G. T. Du, J. Phys. D **42**, 235101 (2009).
14. Y. F. Li, B. Yao, R. Deng, B. H. Li, Z. Z. Zhang, C. X. Shan, D. X. Zhao, and D. Z. Shen, J. Alloys Compd. **575**, 233 (2013).
15. H. Shen, C. X. Shan, J. S. Liu, B. H. Li, Z. Z. Zhang, and D. Z. Shen, Phys. Status Solidi B **250**, 2102 (2013).
16. F. Sun, C. X. Shan, B. H. Li, Z. Z. Zhang, D. Z. Shen, Z. Y. Zhang, and D. Fan, Opt. Lett. **36**, 499 (2011).
17. F. Sun, C. X. Shan, S. P. Wang, B. H. Li, Z. Z. Zhang, C. L. Yang, and D. Z. Shen, Mater. Chem. Phys. **129**, 27 (2011).
18. H. Shen, C. X. Shan, B. H. Li, B. Xuan, and D. Z. Shen, Appl. Phys. Lett. **103**, 232112 (2013).
19. J. Shatma, T. Gora, J. D. Rimstidt, and R. Staley, Chem. Phys. Lett. **15**, 232 (1972).
20. X. H. Wang, B. Yao, Z. P. Wei, D. Z. Shen, Z. Z. Zhang, B. H. Li, Y. M. Lu, D. X. Zhao, J. Y. Zhang, X. W. Fan, L. X. Guan, and C. X. Cong, J. Phys. D **39**, 4568 (2006).
21. J. P. Contour, A. Salesse, M. Froment, M. Garreau, J. Thevenin, and D. Warin, J. Microsc. Spectrosc. Electron. **4**, 483 (1979).
22. P. Fons, K. Iwata, A. Yamada, K. Matsubara, S. Niki, K. Nakahara, T. Tanabe, and H. Takasu, Appl. Phys. Lett. **77**, 1801 (2000).
23. S. M. Sze, *Physics of Semiconductor Devices*, 2nd ed. (Wiley, 1981), p. 25.
24. C. H. Park, S. B. Zhang, and S. H. Wei, Phys. Rev. B **66**, 073202 (2002).
25. J. S. Liu, C. X. Shan, H. Shen, B. H. Li, Z. Z. Zhang, L. Liu, L. G. Zhang, and D. Z. Shen, Appl. Phys. Lett. **101**, 011106 (2012).
26. H. Long, S. Z. Li, X. M. Mo, H. N. Wang, H. H. Huang, Z. Chen, Y. P. Liu, and G. J. Fang, Appl. Phys. Lett. **103**, 123504 (2013).
27. X. Y. Liu, C. X. Shan, C. Jiao, S. P. Wang, H. F. Zhao, and D. Z. Shen, Opt. Lett. **39**, 422 (2014).
28. Z. F. Shi, Y. T. Zhang, J. X. Zhang, H. Wang, B. Wu, X. P. Cai, X. J. Cui, H. W. Liang, B. L. Zhang, and G. T. Du, Appl. Phys. Lett. **103**, 021109 (2013).
29. Y. Liu, C. R. Gorla, S. Liang, N. Emanetoglu, Y. Lu, H. Shen, and M. Wraback, J. Electron. Mater. **29**, 69 (2000).
30. Z. Q. Xu, H. Deng, J. Xie, Y. Li, and X. T. Zu, Appl. Surf. Sci. **253**, 476 (2006).
31. R. Ghosh and D. Basak, Appl. Phys. Lett. **90**, 243106 (2007).
32. J. Zhou, Y. D. Gu, Y. F. Hu, W. J. Mai, P. H. Yeh, G. Bao, A. K. Sood, D. L. Polla, and Z. L. Wang, Appl. Phys. Lett. **94**, 191103 (2009).